# Observation of superradiant bursts in waveguide QED

Christian Liedl, Felix Tebbenjohanns, Constanze Bach, Sebastian Pucher,<sup>†</sup> Arno Rauschenbeutel, and Philipp Schneeweiss\* Department of Physics, Humboldt-Universität zu Berlin, 10099 Berlin, Germany (Dated: November 17, 2022)

Dicke superradiance describes the collective decay dynamics of a fully inverted ensemble of two-level atoms. There, the atoms emit light in the form of a short, intense burst due to a spontaneous synchronization of the atomic dipoles. Typically, to observe this phenomenon, the atoms must be placed in close vicinity of each other. In contrast, here we experimentally observe superradiant burst dynamics with a one-dimensional ensemble of atoms that extends over thousands of optical wavelengths. This is enabled by coupling the atoms to a nanophotonic waveguide, which mediates long-range dipole-dipole interactions between the emitters. The burst occurs above a threshold atom number, and its peak power scales faster with the number of atoms than in the case of standard Dicke superradiance. Moreover, we study the coherence properties of the burst and observe a sharp transition between two regimes: in the first, the phase coherence between the atoms is seeded by the excitation laser. In the second, it is seeded by vacuum fluctuations. Our results shed light on the collective radiative dynamics of spatially extended ensembles of quantum emitters and may turn out useful for generating multi-photon Fock states as a resource for quantum technologies.

#### I. INTRODUCTION

The spontaneous synchronization of individually random processes plays an important role in many natural phenomena, in fields ranging from biology to condensed matter physics [1]. In quantum optics, a paradigmatic example of such synchronization is given by superradiance [2, 3]. There, an ensemble of initially excited atoms emits light in a short, so-called superradiant burst. The latter is characterized by an initial increase of the emitted power, which is due to a spontaneous synchronization of the initially independent atomic dipoles. For this synchronization to occur, the atoms have to emit their radiation into common optical modes. This can, e.g., be ensured by locating all atoms in a volume that is small compared to the wavelength of the optical transition cubed. Alternatively, one can place the atoms in a high-Finesse cavity, thereby relaxing the requirement of tight spatial confinement. Using these two approaches, seminal experiments have been carried out in the last decades, enabled by an ever-increasing level of control of the system parameters [4–9]. The situation is more complex for extended ensembles in free space, since the synchronization via the shared optical mode competes with decay into independent modes [10–17]. It then turns out that superradiant burst dynamics disappears when the atoms are separated in free space by more than an optical wavelength [12]. Recently, major experimental and theoretical effort has been geared towards understanding and controlling the dynamics of quantum emitters that are coupled to waveguides, giving rise to a novel research field termed waveguide quantum electrodynamics (wQED) [18].

There, the waveguide mediates long-range dipole-dipole interactions between the emitters, which can be engineered to be almost unidirectional [19]. These unique interactions make the study of collective radiative effects in wQED an especially intriguing research direction [20–27]. However, reaching the regime of superradiant burst dynamics has remained elusive in wQED so far.

Here, we observe superradiant burst dynamics with about 1000 atoms that are coupled to a nanophotonic waveguide. The coupling is unidirectional, thereby realizing a cascaded quantum system with waveguidemediated long-range interactions. This means that each atom is only driven by the light emitted by the atoms that are further upstream in the cascade. We observe that a superradiant burst only occurs when the number of atoms is larger than a certain threshold Beyond this threshold, the peak power that is emitted into the waveguide increases faster than quadratic with the number of atoms, where quadratic scaling would be expected in the standard case of Dicke superradiance [2, 3]. We also analyze the burst dynamics as a function of the initial state of the atomic ensemble. Our observations are accurately described by the predictions of a cascaded interaction model, whose computational complexity scales only linearly with the number of atom. Finally, we experimentally show that, for a fully inverted ensemble, the superradiant burst exhibits a random phase with respect to the laser. This gives evidence that the build-up of coherence is indeed triggered by vacuum fluctuations. As in the case studied by Dicke, the emergent macroscopic coherence that underlies the superradiant burst in our case thus stems from spontaneous phase locking of the atoms during their decay.

<sup>&</sup>lt;sup>†</sup> Present address: Max-Planck-Institut für Quantenoptik, Hans-Kopfermann-Straße 1, 85748 Garching, Germany

<sup>\*</sup> philipp.schneeweiss@hu-berlin.de

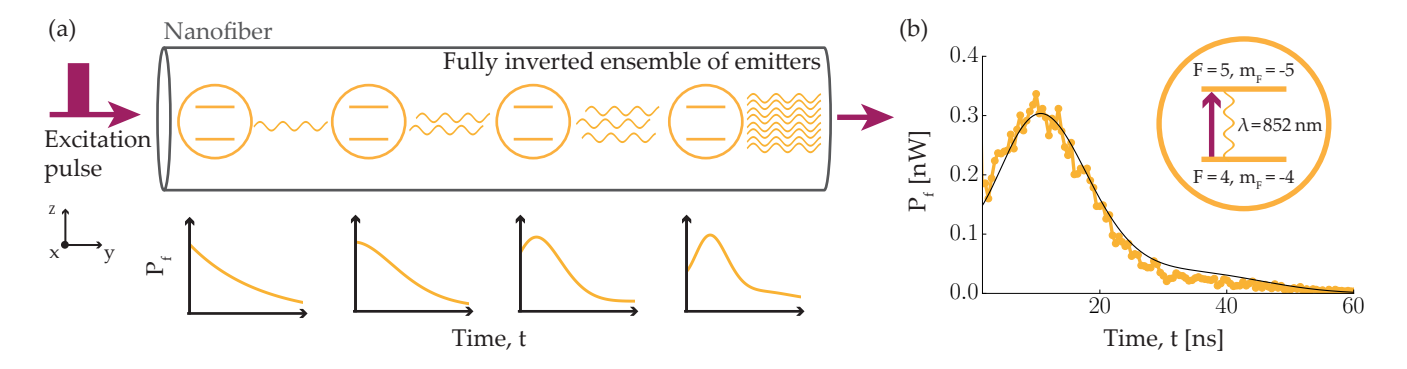


FIG. 1. (a) Schematic representation of the build-up of a superradiant burst in a cascaded system. Cesium atoms (yellow circles) are unidirectionally coupled to the evanescent field of the forward-propagating nanofiber-guided mode (+y-direction). This realizes a cascaded quantum system in which each atom is only driven by the light radiated by upstream atoms, i.e., by atoms shown further to the left. (b) We coherently inverted an ensemble of about 1000 atoms using a short, fiber-guided optical pulse (purple arrow). As the ensemble decays, a superradiant burst establishes along the atomic ensemble, which we observe by detecting the power of the light emitted into the forward-propagating mode,  $P_f$ . The solid black line represents the prediction of our cascaded interaction model.

#### II. EXPERIMENTAL SETUP

A schematic of the experimental setup is shown in Fig. 1(a). We optically interface cesium atoms with the evanescent field surrounding an optical nanofiber, which is realized as the waist of a tapered optical fiber with a nominal diameter of 500 nm. Using nanofiber-guided light, we realize a two-color optical dipole trap that features two diametral arrays of trapping sites for the atoms, located about 230 nm from the fiber surface. We probabilistically load atoms into this trapping potential from a magneto-optical trap [28]. Due to the collisional blockade effect, the maximum number of atoms per trapping site is limited to one [29, 30]. We then apply a magnetic offset field of about 0.5 G in the z-direction. We prepare atoms in only one of the two diametral arrays of trapping sites via side-selective degenerate Raman cooling (DRC) with a fiber-guided laser field that is near-resonant with the  $|6S_{1/2}, F=4\rangle \rightarrow |6P_{3/2}, F=5\rangle$  D2-transition. This cools the atoms on one side of the fiber and heats out atoms on the other side [31]. We infer the number of trapped atoms, N, via transmission spectroscopy [28, 32] and then switch to DRC with a free-space laser beam that is near-resonant with the  $|6S_{1/2}, F=4\rangle \rightarrow |6P_{1/2}, F=4\rangle$ D1-transition. Since the corresponding scattering rate is much smaller than the collective decay rate of the atomic ensemble, we can continuously cool the atoms for the remainder of the experimental sequence without disturbing the atomic dynamics. Thanks to the continuous cooling, not more than 15 % of the atoms are lost during the probing sequence with a duration of 80 ms. In addition to cooling the atoms, our DRC scheme prepares the atoms in their outermost Zeeman ground state,  $|g\rangle = |6S_{1/2}, F = 4, m_F = -4\rangle.$ 

We then excite the atomic ensemble to the  $|e\rangle=|6P_{3/2},F=5,m_F=-5\rangle$  state using a 4 ns-long fiber-guided optical pulse that is much shorter than the ex-

cited state lifetime of about 30 ns [33]. The excitation laser field is locally  $\sigma^-$ -polarized [34, 35] and resonant with the  $|g\rangle \rightarrow |e\rangle$  transition. We recently showed that this technique allows us to almost fully invert ensembles with up to 1000 atoms, with an excited state probability of about 80 % [26]. After the excitation pulse, we measure the power of the waveguide-coupled fluorescence that is emitted into the forward-propagating mode,  $P_f$ , see Supplemental Material [32]. Since the emitted light is  $\sigma^-$ -polarized, the probability that a single atom emits into the locally almost perfectly  $\sigma^-$ -polarized forwardpropagating mode,  $\beta_f \approx 0.01$ , is about ten times larger than the probability for backward emission,  $\beta_b$  [35]. To obtain sufficient counting statistics, we excite the atoms 400 times per sequence at a repetition rate of 5 kHz and average the recorded data over several thousand se-

In Fig. 1(b), we show an example time trace of  $P_f$  as yellow dots. The excitation pulse is switched off at time t=0 ns. Subsequently, the ensemble of about 1000 inverted atoms decays, and we observe an initial increase of  $P_f$ . The power reaches a maximum value of  $P_f^{\rm max}$  after a delay of  $t_{\rm D}\approx 9$  ns, and then decreases. This is in stark contrast to the exponential decay of independent atoms, where the emitted power is monotonically decreasing. The initial increase of the emitted power, as observed in Fig. 1(b), is the characteristic feature of a superradiant burst. This observation evidences that the atomic dipoles synchronize during their decay despite their large separation. This synchronization is facilitated by unidirectional long-range dipole-dipole interactions between all atoms, which are mediated by the nanofiber-guided mode.

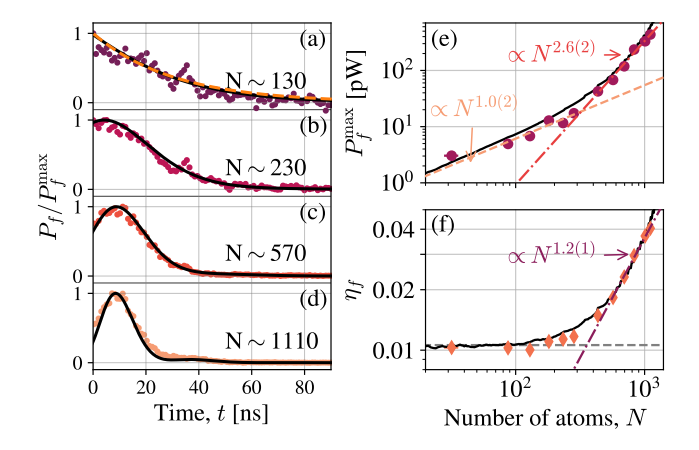


FIG. 2. Scaling of the superradiant burst with the number of atoms, N, which are initially inverted. (a)-(d) Decay dynamics of the power emitted by an inverted ensemble for different N. As we increase N, the dynamics changes from a monotonous decay to a superradiant burst. (e) Scaling of the peak emitted power,  $P_{\text{max}}$ , with N (purple dots). We observe a linear scaling for small N (orange dashed line), which becomes superlinear when the number of atoms in the ensemble exceeds a threshold of about 300 (red dash-dotted line), consistent with the qualitative change of the dynamics in (a)–(d). (f) Scaling of the fraction of absorbed energy emitted into the forward-propagating mode,  $\eta_f$  (orange diamonds). Also here, we observe a threshold in the atom number, beyond which the scaling with N changes from constant to approximately linear. The corresponding model predictions are shown as solid black lines.

#### III. SCALING WITH THE NUMBER OF ATOMS

The spontaneous synchronization of the atomic dipoles in our experiment is in competition with dephasing and with decay into other modes [3]. As a result, the superradiant burst only occurs when the number of atoms exceeds a certain threshold, beyond which spontaneous synchronization dominates. In order to study this threshold behavior, we measure the decay of fully inverted ensembles consisting of different atom numbers, see Fig. 2(a)-(d). For the about 130 inverted atoms in (a), we observe an exponential decay of the power,  $P_f$ , identical to the case of independently emitting atoms, see dashed orange line. As we increase the atom number to about 230 in (b), we first observe a plateau before the emitted power eventually decreases, indicating that the system is close to the onset of a superradiant burst. For 570 atoms, a clear burst becomes apparent, which becomes even more pronounced for 1110 atoms.

From these measurements, we extract the peak emitted power,  $P_f^{\max}$ , and plot it as a function of the atom number N in Fig. 2(e). Two regimes are clearly visible: for small atom numbers,  $P_f^{\max}$  increases linearly with N, and a power-law fit reveals an exponent of 1.0(2). In this regime, the peak emitted power occurs directly after

switching off the excitation laser (t=0 ns). Since all atoms emit independently, the power is given by  $P_f^{\rm max}=P_f(t=0)=\beta_f\Gamma E_{\rm st}$ , where  $E_{\rm st}\approx N\hbar\omega$  is the energy stored in the ensemble after the excitation pulse. This energy is radiated into the forward-propagating mode with a rate  $\beta_f\Gamma$ , where  $\Gamma/(2\pi)\approx 5.22$  MHz is the excited state decay rate. As N is increased further, the scaling changes and the extracted exponent becomes 2.6(2). This threshold behavior and the superlinear scaling are indicative of a synchronization of the atomic dipoles, which leads to a faster emission of the stored energy such that  $P_f^{\rm max}$  exceeds  $\beta_f\Gamma E_{\rm st}$ . Indeed, the change of scaling in  $P_f^{\rm max}$  is accompanied by the occurrence of burst dynamics, see Fig. 2(c) and (d).

In the textbook case of the emission of a Dicke-like superradiant burst by a strongly confined ensemble, the scaling is quadratic since each atom constructively adds to the macroscopic dipole moment of the ensemble, and the power is proportional to its square [2]. There, the atoms exclusively couple to a single mode, such that the entire energy stored in the ensemble,  $E_{\rm st}$ , is emitted into this mode, irrespective of whether the dipoles synchronize or not. However, in our experiment, a single atom emits only about 1% of its radiation into the guided mode and about 99% of the light is scattered into the free-space modes. During the collective decay of the atoms, a phase pattern is formed across the atomic dipoles, which leads to constructive interference into the forward-propagating mode. Therefore, the atoms emit into a narrower solid angle as N increases. Accordingly, a larger fraction of the radiated power is collected by the aperture of the nanofiber-guided mode. This explains the faster-thanquadratic scaling beyond the threshold value observed in our experiment. In order to confirm our interpretation, we analyze the collective enhancement of forward scattering by measuring the fraction of the stored energy that is emitted into the forward-propagating mode,  $\eta_f$  [26]. We plot the experimentally determined  $\eta_f$  as a function of the atom number, N, in Fig. 2(f) and find a similar threshold behavior as for the peak emitted power,  $P_f^{\text{max}}$ . For small N,  $\eta_f$  stays at a constant value of about  $0.01 \approx \beta_f$ , as expected for independently emitting atoms, see dashed gray line in Fig. 2(f). For larger atom numbers,  $\eta_f$  increases as  $N^{1.2(1)}$ , i.e., forward scattering is indeed collectively enhanced compared to independent decay. We note that this mechanism is fundamentally different from the case of coherent forward scattering in the weak excitation regime, where a similar phase pattern is imprinted on the ensemble by the exciting laser field [24, 36].

# IV. SUPERRADIANT BURST DYNAMICS FOR A FINITE INITIAL DIPOLE

We now explore the dynamics of the superradiant burst for different initial states of the atomic ensemble. By exciting the atoms with short, resonant optical pulses of

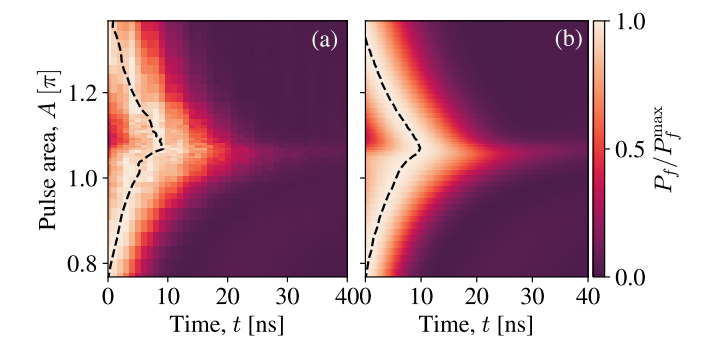


FIG. 3. Dynamics of the power emitted into the nanofiberguided mode,  $P_f$ , for different pulse areas seen by the first atom, A. Each time trace is normalized by its peak value,  $P_f^{\text{max}}$ . The time at which the maximum is reached,  $t_D$ , is indicated by the black dashed lines. (a) shows the measured data, while (b) shows the corresponding model predictions.

varying power and, correspondingly, different pulse areas, A, we prepare each atom close to a coherent superposition of ground and excited state [26]:

$$|\psi\rangle = \cos\left(\frac{A}{2}\right)|g\rangle - i\sin\left(\frac{A}{2}\right)|e\rangle,$$
 (1)

where we have chosen a rotating frame that moves with the forward-propagating laser mode. The time traces of the emitted power,  $P_f$ , are shown in Fig. 3(a), where each time trace is normalized by its peak value,  $P_f^{\text{max}}$ . We extract the time at which the maximal power is emitted into the nanofiber,  $t_{\rm D}$ , for each time trace and display it as the black dashed line. A delay time of  $t_{\rm D} > 0$  indicates the occurrence of a superradiant burst. For small pulse areas  $(A < 0.8\pi)$ , the power decreases monotonously as the ensemble decays, yielding zero delay,  $t_D = 0$ . However, when A is close to  $\pi$ , and the ensemble is substantially inverted, a superradiant burst is apparent. The closer the ensemble is to full inversion, the larger the delay  $t_{\rm D}$ , with a maximal value of  $t_D \approx 9$  ns. When A is further increased, the ensemble is coherently de-excited and the burst gradually vanishes. This observation confirms that we can excite the regime close to full inversion in a controlled manner.

We observe the largest delay, and thus, full inversion, for a pulse area of  $A=1.07~\pi$ , i.e. slightly larger than  $\pi$ . In addition, we observe a slight asymmetry of the time traces with respect to full inversion. Both effects are a consequence of the finite absorption of the excitation pulse along the ensemble and the cascaded interaction, which we checked numerically, see Supplemental Material [32]. In Fig. 3(b), we show the corresponding model prediction and find quantitative agreement, confirming that our cascaded interaction model captures the essential physical mechanism which determines the system dynamics.

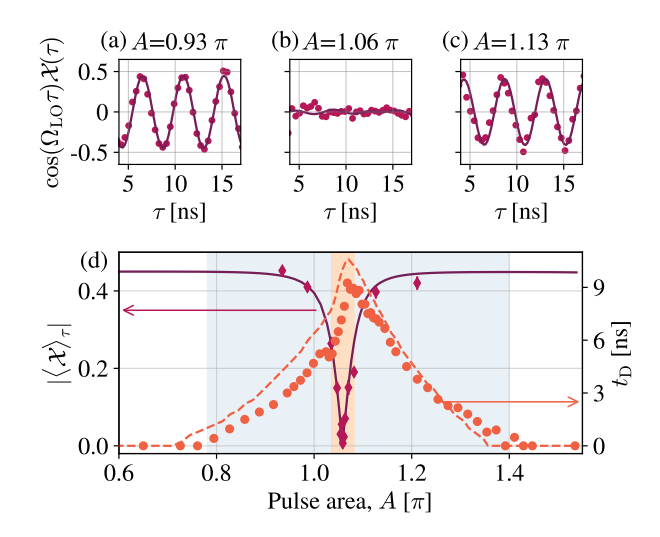


FIG. 4. Analysis of the coherence of the fluorescent light using heterodyne detection. (a)–(c) First order cross correlation between the excitation laser and the light emitted into the forward-propagating mode,  $\mathcal{X}(\tau)$ , oscillating at the local oscillator detuning,  $\Omega_{\text{LO}}$ , for different pulse areas, A. When maximal inversion is reached, see (b), the oscillations disappear, indicating that there is no fixed phase relationship between fluorescence and excitation laser. (d) Averaged magnitude of the coherence with respect to the laser,  $|\langle \mathcal{X} \rangle_{\tau}|$ , for different A, see purple diamonds, and time delay of the superradiant burst,  $t_{\text{D}}$ , see orange dots.

#### V. COHERENCE PROPERTIES

To further understand the role of coherence in the formation of the superradiant burst in our system, we superpose the light emitted into the forward-propagating mode with a local oscillator that is derived from the excitation laser and detuned by  $\Omega_{\rm LO} = 2\pi \times 230$  MHz. From the intensity-intensity correlations of the resulting heterodyne signal, we infer the first-order coherence function of the light exiting the nanofiber,  $g^{(1)}(t, t+\tau)$ , which is modulated with the local oscillator detuning,  $\Omega_{LO}$ , see Supplemental Material [32]. We plot the result of this analysis in Fig. 4 for different pulse areas, A. The corresponding model predictions are shown as solid lines. In panels (a)-(c), we show  $\mathcal{X}(\tau) = g^{(1)}(t = -2 \text{ ns}, t + \tau)$ , which is modulated at the local oscillator detuning. Since the signal at time t=-2 ns is dominated by the transmitted excitation laser light,  $\mathcal{X}(\tau)$  effectively measures the first order cross correlation between the excitation laser light and the light emitted by the atoms. In panel (a), the atoms are not yet fully inverted  $(A = 0.93 \pi)$ , and we observe an oscillation with large visibility. This indicates that the emitted light is coherent with the laser. We extrapolate that  $\mathcal{X}(\tau = 0 \text{ ns})$  is negative, meaning that the light emitted by the atoms is phase shifted by  $\pi$ with respect to the laser. This is expected for pulse areas smaller than  $\pi$ , since the field radiated by the induced

atomic dipoles oscillates  $\pi$  out of phase with the excitation laser, see Supplemental Material [32]. Similarly, we observe large visibility in (c), however with opposite phase, i.e.,  $\mathcal{X}(\tau = 0 \text{ ns})$  is positive. This is due to the fact that the atomic dipole switches sign for a pulse area larger than  $\pi$ . Importantly, however, for maximal inversion in (b), we do not observe interference, i.e. the visibility of the interference fringes is practically zero. This demonstrates that the emitted light is incoherent with respect to the excitation laser field, i.e., the observed superradiant burst is triggered by vacuum fluctuations that have a random phase with respect to the excitation laser. In order to quantify the residual coherence with respect to the excitation laser, we repeat the measurement shown in Figs. 4(a)–(c) for even more pulse areas, A. We fit the function  $C\cos(\Omega_{\rm LO}t)$  to the data, with only the amplitude C as a free parameter. The latter thus corresponds to the magnitude of  $\mathcal{X}(\tau)$  averaged over  $\tau$ . Its modulus quantifies the average coherence of the emitted light with respect to the excitation laser, and is plotted as purple diamonds in Fig. 4(d). The corresponding model prediction is shown as the solid purple line. We also plot the time  $t_D$  at which the peak power  $P_t^{\text{max}}$  is emitted together with the model predictions. Note that this is the same data shown as a black dashed line in Fig. 3(a). We observe that the minimum of  $|\langle \mathcal{X} \rangle_{\tau}|$  appears when the delay  $t_{\rm D}$  is longest, i.e., when the ensemble is maximally inverted. Interestingly, the coherence with respect to the laser features a dip which is much narrower than the region in which  $t_{\rm D}$  is larger than zero. This allows us to identify two regimes of superradiant burst dynamics in our experiment. First, in the light-red shaded area, the superradiant burst is incoherent with respect to the laser and therefore triggered by vacuum fluctuations, sometimes called superfluorescence [37]. Second, in the lightblue shaded regions, a burst appears, which is coherent with the excitation laser. Here, the phase synchronization is not spontaneous, but the phase is imprinted onto the ensemble by the excitation laser field.

# VI. NUMERICAL MODEL

Understanding this collective dynamics quantitatively usually involves solving the many-body master equation [38]. However, since the size of the corresponding Hilbert space scales exponentially with the number of atoms, a numerical solution is prohibitive for ensembles of hundreds of emitters. In contrast, here we present a model whose computational complexity scales only linearly in the number of atoms. It is an extension of the cascaded interaction model presented in Ref. [26], and its predictions are in quantitative agreement with our data, see Figs. 1–4. Owing to the unidirectional atom-waveguide coupling present in our system, the atoms emit almost exclusively into the forward-propagating mode, i.e.,  $\beta_f \gg \beta_b$  [35]. Therefore, we model our system as a cascaded quantum system, in which the dynamics of

each atom only depends on the light emitted by upstream atoms [39, 40]. Due to the large average separation between the atoms (larger than an optical wavelength), we furthermore neglect free-space dipole-dipole interactions. In this cascaded interaction model, the  $k^{\text{th}}$  atom is described by the spin operator,  $\hat{\sigma}_k = |g\rangle_k \langle e|_k$ , and is driven by the input field operator,  $\hat{a}_k(t)$ . The output field is connected to the next atom's input,  $\hat{a}_{k+1}(t)$ , and is given by the input-output equation [41]

$$\hat{a}_{k+1}(t) = \hat{a}_k(t) - i\sqrt{\beta_f \Gamma} \hat{\sigma}_k. \tag{2}$$

The dynamics of the spin operator is determined by the quantum Langevin equation

$$\frac{\mathrm{d}}{\mathrm{d}t}\hat{\sigma}_{k} = -\frac{\Gamma}{2}\hat{\sigma}_{k} - \mathrm{i}\sqrt{\beta\Gamma}\left(1 - 2\hat{\sigma}_{k}^{\dagger}\hat{\sigma}_{k}\right)\hat{a}_{k}(t). \tag{3}$$

If the input is in a coherent state  $\alpha_k(t) = \langle \hat{a}_k(t) \rangle$  (such as for the first atom), the Langevin equation reduces to the optical Bloch equations. Generally, it is well known that the output field  $\hat{a}_{k+1}$  is not in a coherent state anymore. In particular, the output power  $P_{k+1} = \hbar \omega \langle \hat{a}_{k+1}^{\dagger} \hat{a}_{k+1} \rangle$  is larger than its coherent part  $P_{k+1}^c = \hbar \omega |\langle \hat{a}_{k+1} \rangle|^2$ , where  $\hbar \omega$  is the photon energy. The difference  $P_{k+1}^{inc} = P_{k+1} - P_{k+1}^c$  is commonly referred to as the "incoherent" or "nonlinear" part of the emitted light due to spontaneously emitted light. Since the system is driven close to inversion in our case, this incoherent part largely exceeds the coherent part  $P_{k+1}^c$ . In order to describe this incoherent driving of the next atom, we model the input field  $\hat{a}_k$  as the superposition of a coherent field and a "randomly-phased laser field" [42] to account for the spontaneous emission. The density operator of such a field is given by

$$\rho_L = \frac{1}{2\pi} \int_0^{2\pi} d\phi \, |\alpha(\phi)\rangle \langle \alpha(\phi)|, \qquad (4)$$

which represents a mixture of coherent states with amplitudes  $\alpha(\phi) = \sqrt{P_k^c} + e^{i\phi} \sqrt{P_k^{\text{inc}}}$ , homogeneously sampled over the phase  $\phi$ . This "mixed coherent state" has the necessary property that its total power  $\langle \hat{a}_k^{\dagger} \hat{a}_k \rangle =$  $P_k^c + P_k^{\text{inc}}$  is larger than its coherent part  $|\langle \hat{a}_k \rangle|^2 = P_k^c$ . Moreover, we can still straight-forwardly solve the atomic dynamics of the  $k^{\text{th}}$  atom given this input state by solving the optical Bloch equation for each phase  $\phi$ . We then numerically compute the output's coherent and incoherent parts  $P_{k+1}^c$  and  $P_{k+1}^{\text{inc}}$ , respectively, by integrating over  $\phi$  [32]. We apply this method iteratively to each atom and finally obtain the output power  $P_f = P_{N+1}$ . In addition, we average the simulated time traces over a truncated Gaussian distribution of  $\beta_f$  values to account for thermal fluctuations of the atomic position relative to the nanofiber surface and fit the corresponding mean and standard deviation to the experimental data, yielding 0.0112 and 0.0065, respectively [32]. Notably, we only need these two free parameters to obtain quantitative agreement with the data throughout the whole parameter

space studied in this work. We numerically checked that the finite width of the excitation pulse and the inhomogeneous spread of coupling strengths does not qualitatively alter the dynamics [32]. The quantitative agreement of our model with the data attests that our system can indeed be modeled as a cascaded quantum system.

### VII. CONCLUSION AND OUTLOOK

We have experimentally observed superradiant burst dynamics of an ensemble of nanofiber-coupled atoms. Our results show that the long-range dipole-dipole interactions inherent to waveguide quantum electrodynamics can be used to access novel regimes of collective radiative dynamics. In particular, our experimental platform features unidirectional photon emission into the waveguide, thereby realizing a cascaded system of quantum emitters. In our experiment, the directionality can be tuned via the choice of the excited atomic state [35]. An interesting future research direction would therefore be to study the dependence of the collective radiative dynamics on the asymmetry of atom-waveguide coupling [43]. Moreover, placing the atoms in a nanofiber-integrated optical resonator would constitute a versatile testbed to study the underlying physical mechanism of a superradiant laser, which could be used as an active optical clock [7, 44]. Furthermore, beyond the results discussed in this manuscript, it would be intriguing to study the long-term dynamics of the superradiant burst emission. In this regime, sub-radiant features related to a high degree of correlations between the atomic dipoles are expected. Finally, our work constitutes a first step towards generating complex quantum states of light using large ensembles of emitters, such as multi-photon Fock states [45], which are highly desirable in quantum metrology [46, 47].

## ACKNOWLEDGMENTS

We thank A. Asenjo García, A. Browaeys, S. Cardenas López, J. I. Cirac, I. Ferrier-Barbut, K. Hammerer, K. Kusmierek, S. Masson, L. A. Orozco, and J. Volz for stimulating discussions and helpful comments. We acknowledge funding by the Alexander von Humboldt Foundation in the framework of the Alexander von Humboldt Professorship endowed by the Federal Ministry of Education and Research.

- [1] S. Strogatz, Sync: The emerging science of spontaneous order (Penguin UK, 2004).
- [2] R. H. Dicke, Coherence in spontaneous radiation processes, Phys. Rev. 93, 99 (1954).
- [3] M. Gross and S. Haroche, Superradiance: An essay on the theory of collective spontaneous emission, Phys. Rep. 93, 301 (1982).
- [4] N. Skribanowitz, I. Herman, J. MacGillivray, and M. Feld, Observation of Dicke superradiance in optically pumped HF gas, Phys. Rev. Lett. 30, 309 (1973).
- [5] M. Gross, C. Fabre, P. Pillet, and S. Haroche, Observation of near-infrared Dicke superradiance on cascading transitions in atomic sodium, Phys. Rev. Lett. 36, 1035 (1976).
- [6] M. Gross, P. Goy, C. Fabre, S. Haroche, and J. Raimond, Maser oscillation and microwave superradiance in small systems of rydberg atoms, Phys. Rev. Lett. 43, 343 (1979).
- [7] J. G. Bohnet, Z. Chen, J. M. Weiner, D. Meiser, M. J. Holland, and J. K. Thompson, A steady-state superradiant laser with less than one intracavity photon, Nature 484, 78 (2012).
- [8] M. A. Norcia, M. N. Winchester, J. R. Cline, and J. K. Thompson, Superradiance on the millihertz linewidth strontium clock transition, Science Adv. 2, e1601231 (2016).
- [9] G. Ferioli, A. Glicenstein, F. Robicheaux, R. T. Sutherland, A. Browaeys, and I. Ferrier-Barbut, Laser-driven superradiant ensembles of two-level atoms near Dicke regime, Phys. Rev. Lett. 127, 243602 (2021).
- [10] L. Ostermann, H. Zoubi, and H. Ritsch, Cascaded collective decay in regular arrays of cold trapped atoms, Opt. Exp. 20 (2012).
- [11] S. J. Masson, I. Ferrier-Barbut, L. A. Orozco, A. Browaeys, and A. Asenjo-Garcia, Many-body signatures of collective decay in atomic chains, Phys. Rev. Lett. 125, 263601 (2020).
- [12] S. J. Masson and A. Asenjo-Garcia, Universality of Dicke superradiance in arrays of quantum emitters, Nat. Comm. 13, 1 (2022).
- [13] E. Sierra, S. J. Masson, and A. Asenjo-Garcia, Dicke superradiance in ordered lattices: dimensionality matters, Phys. Rev. Res. 4, 023207 (2022).
- [14] F. Robicheaux, Theoretical study of early-time superradiance for atom clouds and arrays, Phys. Rev. A 104, 063706 (2021).
- [15] O. Rubies-Bigorda and S. F. Yelin, Superradiance and subradiance in inverted atomic arrays, arXiv:2110.11288 (2021)
- [16] B. Lemberger and K. Mølmer, Radiation eigenmodes of Dicke superradiance, Phys. Rev. A 103, 033713 (2021).
- [17] D. Plankensteiner, C. Hotter, and H. Ritsch, Quantum-cumulants. jl: A Julia framework for generalized mean-field equations in open quantum systems, Quantum 6, 617 (2022).
- [18] A. S. Sheremet, M. I. Petrov, I. V. Iorsh, A. V. Poshakinskiy, and A. N. Poddubny, Waveguide quantum electrodynamics: collective radiance and photon-photon correlations, arXiv preprint arXiv:2103.06824 (2021).
- [19] P. Lodahl *et al.*, Chiral quantum optics, Nature **541**, 473 (2017).

- [20] A. Goban, C.-L. Hung, J. D. Hood, S.-P. Yu, J. A. Muniz, O. Painter, and H. J. Kimble, Superradiance for atoms trapped along a photonic crystal waveguide, Phys. Rev. Lett. 115, 063601 (2015).
- [21] P. Solano, P. Barberis-Blostein, F. K. Fatemi, L. A. Orozco, and S. L. Rolston, Super-radiance reveals infinite-range dipole interactions through a nanofiber, Nat. Commun. 8, 1 (2017).
- [22] N. V. Corzo, J. Raskop, A. Chandra, A. S. Sheremet, B. Gouraud, and J. Laurat, Waveguide-coupled single collective excitation of atomic arrays, Nature 566, 359 (2019).
- [23] J. Kumlin, K. Kleinbeck, N. Stiesdal, H. Busche, S. Hofferberth, and H. P. Büchler, Nonexponential decay of a collective excitation in an atomic ensemble coupled to a one-dimensional waveguide, Phys. Rev. A 102, 063703 (2020).
- [24] R. Pennetta, D. Lechner, M. Blaha, A. Rauschenbeutel, P. Schneeweiss, and J. Volz, Observation of coherent coupling between super-and subradiant states of an ensemble of cold atoms collectively coupled to a single propagating optical mode, arXiv:2112.10806 (2021).
- [25] R. Pennetta, M. Blaha, A. Johnson, D. Lechner, P. Schneeweiss, J. Volz, and A. Rauschenbeutel, Collective radiative dynamics of an ensemble of cold atoms coupled to an optical waveguide, Phys. Rev. Lett. 128, 073601 (2022).
- [26] C. Liedl, S. Pucher, F. Tebbenjohanns, P. Schneeweiss, and A. Rauschenbeutel, Collective excitation and decay of waveguide-coupled atoms: from timed Dicke states to inverted ensembles, arXiv:2204.04106 (2022).
- [27] A. Tiranov, V. Angelopoulou, C. J. van Diepen, B. Schrinski, O. A. D. Sandberg, Y. Wang, L. Midolo, S. Scholz, A. D. Wieck, A. Ludwig, et al., Coherent superand subradiant dynamics between distant optical quantum emitters, arXiv:2210.02439 (2022).
- [28] E. Vetsch, D. Reitz, G. Sagué, R. Schmidt, S. Dawkins, and A. Rauschenbeutel, Optical interface created by laser-cooled atoms trapped in the evanescent field surrounding an optical nanofiber, Phys. Rev. Lett. 104, 203603 (2010).
- [29] N. Schlosser, G. Reymond, and P. Grangier, Collisional blockade in microscopic optical dipole traps, Phys. Rev. Lett. 89, 023005 (2002).
- [30] E. Vetsch, S. T. Dawkins, R. Mitsch, D. Reitz, P. Schneeweiss, and A. Rauschenbeutel, Nanofiber-based optical trapping of cold neutral atoms, IEEE Journal of Selected Topics in Quantum Electronics 18, 1763 (2012).
- [31] Y. Meng, A. Dareau, P. Schneeweiss, and A. Rauschenbeutel, Near-ground-state cooling of atoms optically trapped 300 nm away from a hot surface, Phys. Rev. X 8, 031054 (2018).
- [32] See Supplemental Material for a more detailed description of the loading of the atom trap, the detection setup, and the theoretical modeling.
- [33] D. A. Steck, Cesium D line data, available at https://steck.us/alkalidata (2019).
- [34] F. L. Kien, J. Liang, K. Hakuta, and V. Balykin, Field intensity distributions and polarization orientations in a vacuum-clad subwavelength-diameter optical fiber, Opt. Commun. 242, 445 (2004).

- [35] R. Mitsch, C. Sayrin, B. Albrecht, P. Schneeweiss, and A. Rauschenbeutel, Quantum state-controlled directional spontaneous emission of photons into a nanophotonic waveguide, Nat. Commun. 5, 1 (2014).
- [36] S. Okaba, D. Yu, L. Vincetti, F. Benabid, and H. Katori, Superradiance from lattice-confined atoms inside hollow core fibre, Commun. Phys. 2, 1 (2019).
- [37] R. Bonifacio and L. Lugiato, Cooperative radiation processes in two-level systems: Superfluorescence, Phys. Rev. A 11, 1507 (1975).
- [38] F. L. Kien and K. Hakuta, Cooperative enhancement of channeling of emission from atoms into a nanofiber, Phys. Rev. A 77, 013801 (2008).
- [39] H. Carmichael, Quantum trajectory theory for cascaded open systems, Phys. Rev. Lett 70, 2273 (1993).
- [40] C. Gardiner, Driving a quantum system with the output field from another driven quantum system, Phys. Rev. Lett. 70, 2269 (1993).
- [41] C. W. Gardiner and M. J. Collett, Input and output in damped quantum systems: Quantum stochastic differential equations and the master equation, Phys. Rev. A 31, 3761 (1985).
- [42] L. Mandel and E. Wolf, Optical Coherence and Quantum Optics (Cambridge University Press, 1995).
- [43] S. Cardenas-Lopez, S. J. Masson, Z. Zager, and A. Asenjo-Garcia, Many-body superradiance and dynamical symmetry breaking in waveguide QED, arXiv:2209.12970 (2022).
- [44] D. Meiser, J. Ye, D. R. Carlson, and M. J. Holland, Prospects for a millihertz-linewidth laser, Phys. Rev. Lett. 102, 163601 (2009).
- [45] A. González-Tudela, V. Paulisch, D. E. Chang, H. J. Kimble, and J. I. Cirac, Deterministic generation of arbitrary photonic states assisted by dissipation, Phys. Rev. Lett. 115, 163603 (2015).
- [46] V. Paulisch, M. Perarnau-Llobet, A. González-Tudela, and J. I. Cirac, Quantum metrology with onedimensional superradiant photonic states, Phys. Rev. A 99, 043807 (2019).
- [47] M. Perarnau-Llobet, A. González-Tudela, and J. I. Cirac, Multimode fock states with large photon number: effective descriptions and applications in quantum metrology, Quantum Sci. Technol. 5, 025003 (2020).

# Supplemental Material: Observation of superradiant bursts in waveguide QED

### A. Loading of the nanofiber-based atom trap

We load cesium atoms into a magneto-optical trap (MOT) and perform optical molasses cooling to transfer the atoms into the nanofiber-based trapping potential, which features two diametral arrays of trapping sites [28]. The trapping potential is created by running-wave blue-detuned nanofiber-guided field (wavelength 760 nm, power 20.5 mW) and a standing-wave red-detuned field (wavelength 1064 nm, total power 2.4 mW). The loading is probabilistic and, due to the collisional blockade effect, each potential minimum is occupied by at most one atom [29]. Then, we apply a homogenous magnetic offset field of about 0.5 G along +z (see Fig. 1 in the main text) and further cool the atoms on one side of the nanofiber by degenerate Raman cooling (DRC) using nanofiber-guided light that is near-resonant with the  $|6S_{1/2}, F=4\rangle \rightarrow |6P_{3/2}, F=5\rangle$ D2 transition [31]. At the same time, the atoms on the other side of the nanofiber are subject to degenerate Raman heating and are expelled from the trap, such that we are left with a one-dimensional array of atoms on only one side of the nanofiber. After these preparatory steps, we switch off both the MOT and DRC lasers fields such that during the subsequent measurements, there is no resonant light at a wavelength of 852 nm, except for the excitation laser. As described in the main text, we then use an additional free-space laser resonant with the D1 transition at a wavelength of 894 nm in order to cool the trapped atoms by DRC. The number of trapped atoms, N, can be tuned by changing the MOT loading time, which ranges from 80 ms to 7 s.

## B. Detection setup

Figure S1 schematically depicts the detection setup that we use to measure the power of the light exiting the waveguide in the forward direction. We first spectrally filter the signal field at a wavelength of 852 nm from the trapping light fields and other background light using a volume Bragg grating. The light is first split up by a 50:50 beam splitter and then further separated by a 10.90 (R:T) beam splitter. To further suppress the background, each beam then passes a bandpass filter that is centered around 852 nm. We detect the light at the different output ports of the beam splitters using two fiber-coupled single photon counting modules (SPCM 1 and SPCM 2) and a fiber-coupled hybrid photodetector (HPD). We use SPCM 1 to measure the probe transmission spectrum, from which we infer the optical depth of the atomic ensemble and the number of trapped atoms. For the experiments shown in the manuscript, we ex-

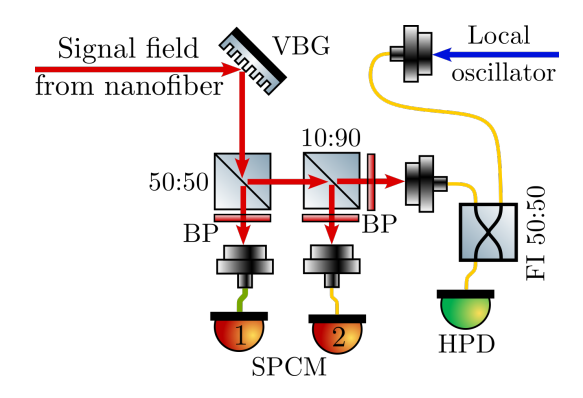


FIG. S1. Schematic of the detection setup. The signal field is spectrally filtered around a wavelength of 852 nm using a volume Bragg grating (VBG) and a bandpass filter (BP) in front of each fiber-coupled detector. The yellow and green lines depict single-mode and multi-mode fibers, respectively. We measure the power of the signal field using two single photon counting modules (SPCM) and a hybrid photodetector (HPD). The light incident on the HPD can be overlapped with a local oscillator using a fiber-integrated 50:50 beam-splitter (FI 50:50). The frequency of the local oscillator field is shifted by 230 MHz with respect to the excitation laser field.

pose the atomic ensemble to intense optical pulses, which have a power that is several orders of magnitude larger than the power emitted by the ensemble during its decay. Since our SPCMs have a dead time of about 25 ns. we have to substantially attenuate the power incident on the SPCMs in order to detect the fluorescence that follows the intense excitation pulse. In contrast, the HPD features a much shorter dead time of only about 2 ns. We can therefore saturate the HPD during the excitation pulse and still detect the fluorescence signal. The signal of the HPD is highly saturated during the excitation pulse. Therefore, we use the signal from SPCM 2 to extract the fraction of absorbed energy that is emitted into the forward direction by the atoms,  $\eta_f$ . To ensure that the excitation pulse does not saturate the signal from SPCM 2, we attenuate the light incident on SPCM 2 using neutral density filters.

For the measurements presented in Sec. V of the main manuscript, we superimpose the signal incident on the HPD with a local oscillator light field using a fiber-integrated 50:50 beam splitter. We derive the local oscillator field from the excitation laser field and shift its frequency by 230 MHz. While performing the heterodyne measurements, we also record the bare signal field (without local oscillator) using SPCM 2. We use the resulting time traces to normalize the first-order coherence function that we extract from the heterodyne signal, see below.

# C. Extraction of the first-order coherence function from the heterodyne signal

The first- and second-order correlation functions of a light field a(t) with power  $P(t) = \langle a^{\dagger}(t)a(t) \rangle$  are defined as:

$$G^{(1)}(t,\tau) = \langle a^{\dagger}(t)a(t+\tau)\rangle,$$

$$g^{(1)}(t,\tau) = \frac{G^{(1)}(t,\tau)}{\sqrt{P(t)P(t+\tau)}},$$

$$G^{(2)}(t,\tau) = \langle a^{\dagger}(t)a^{\dagger}(t+\tau)a(t+\tau)a(t)\rangle,$$

$$g^{(2)}(t,\tau) = \frac{G^{(2)}(t,\tau)}{P(t)P(t+\tau)}.$$
(S1)

Here,  $g^{(1)}$  and  $g^{(2)}$  denote the normalized first-order and second-order correlation functions, respectively. Let us assume a light field a(t) with power P(t) that describes the nanofiber-guided mode and superpose a classical, continuous-wave local oscillator field  $a_{lo}$  with power  $P_{LO}$ , with a randomly fluctuating relative phase,  $\theta_{LO}$ , and relative frequency,  $\omega_{LO}$ :

$$a_{lo}(t) = \sqrt{P_{LO}} e^{i(\omega_{LO}t + \theta_{LO})}.$$
 (S2)

The field and power incident on the detector are then given by

$$a_D(t) = \sqrt{P_{\text{LO}}} e^{i(\omega_{\text{LO}}t + \theta_{\text{LO}})} + a(t),$$
 (S3)

$$P_D(t) = P_{LO} + P(t). \tag{S4}$$

In our experiment, we measure the normalized secondorder correlation function of this heterodyne signal. We average over the relative phase between local oscillator and the signal field,  $\theta_{LO}$ , since the latter is not stabilized and drifts randomly on the time scale of the repetition period of our measurements. Due to these random drifts, there is no interference term in Eq. (S4) since it averages to zero. Using the definitions in Eqs. (S1), we obtain the normalized second-order autocorrelation function of the heterodyne signal,

$$g_D^{(2)}(t,\tau) = 1 + \frac{2P_{\text{LO}}\sqrt{P(t)P(t+\tau)}}{P_D(t)P_D(t+\tau)}\cos(\omega_{\text{LO}}\tau)g^{(1)}(t,\tau) + \frac{P(t)P(t+\tau)}{P_D(t)P_D(t+\tau)}[g^{(2)}(t,\tau) - 1].$$
(S5)

Note that, since we drive the atomic ensemble on resonance, we assume that  $g^{(1)}$  is real, which is confirmed by our theoretical model. Since, for the experimental parameters in our experiment,  $P_{\text{LO}} \gg \sqrt{P(t)P(t+\tau)}$ , we neglect the last term that includes the contribution of  $g^{(2)}(t,\tau)$  such that we are left with

$$g_D^{(2)}(t,\tau) = 1 + V_{\text{max}}(t,\tau)\cos(\omega_{\text{LO}}\tau)g^{(1)}(t,\tau).$$
 (S6)

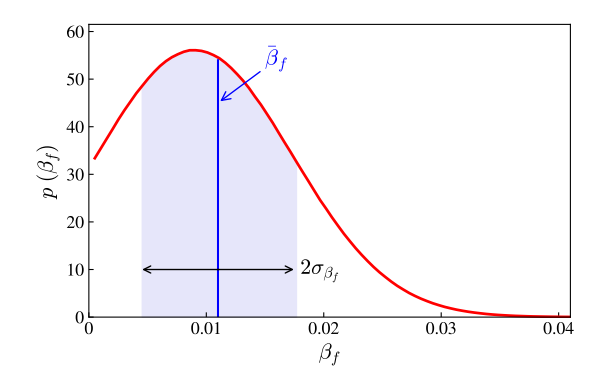


FIG. S2. Probability distribution used to model temperature-induced fluctuations of the atom-waveguide coupling strength,  $\beta_f$ . The fitted mean value,  $\bar{\beta}_f = 0.0112$ , and the standard deviation,  $\sigma_{\beta_f} = 0.0065$ , of the truncated Gaussian distribution are shown as the blue vertical line and black double arrow, respectively.

Here, we have introduced the maximum visibility of  $V_{\text{max}}(t,\tau)$ .

$$V_{\text{max}}(t,\tau) = \frac{2P_{\text{LO}}\sqrt{P(t)P(t+\tau)}}{P_D(t)P_D(t+\tau)}.$$
 (S7)

The second-order correlation function of our heterodyne signal is thus given by the first-order correlation function of the signal field a(t), oscillating at  $\omega_{\rm LO}$ . We extract both  $g_D^{(2)}(t,\tau)$  and  $V_{\rm max}(t,\tau)$  from our measurements and infer the following quantity from our data:

$$\cos(\omega_{lo}\tau)g^{(1)}(t,\tau) = \frac{g_D^{(2)}(t,\tau) - 1}{V_{max}(t,\tau)},$$
 (S8)

which we show in Fig. 4 of the manuscript. Due to an imperfect overlap between the polarizations of the signal field and the local oscillator field, the maximal visibility in the experiment is further reduced. We experimentally checked that the oscillations shown in Fig. 4 of the main manuscript indeed reach maximal contrast if a polarization filter is introduced in front of the detector.

# D. Fluctuations of the coupling strength due to temperature

Since the atoms couple to the evanescent field of the nanofiber-guided mode, the coupling strength of each atom depends on its radial distance from the nanofiber surface. Due to the finite temperature of the atoms in the traps, this radial distance, and consequently, the atom-waveguide coupling strength,  $\beta_f$ , fluctuates. Moreover, the 400 excitation pulses sent per experimental sequence slightly heat the atoms during the course of the measurements. We note that, while the coupling strength fluctuates from one experimental realization to

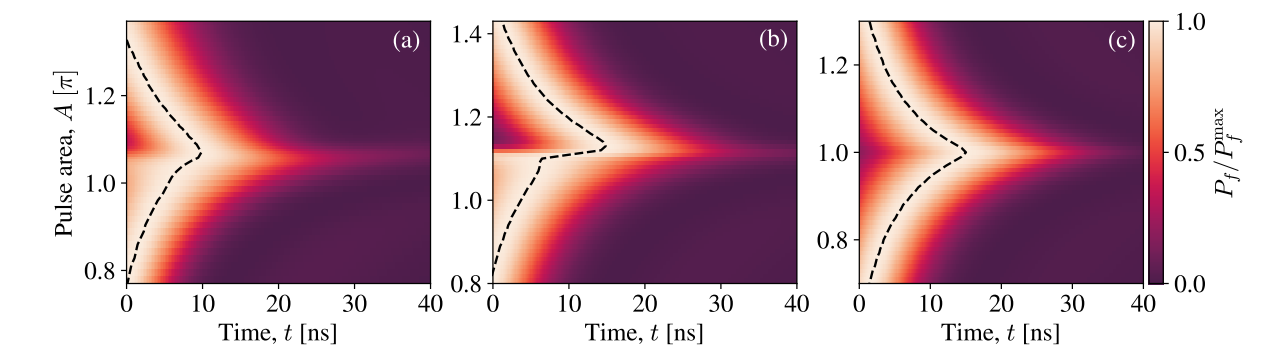


FIG. S3. Comparison of different model predictions for the dynamics of the power emitted into the forward-propagating mode,  $P_f$ , as a function of the pulse area seen by the first atom, A. Each time trace is normalized by its peak value,  $P_f^{\max}$ . (a) We assume both fluctuating coupling strengths and a finite excitation pulse duration. (b) We assume constant coupling strengths and a finite excitation pulse duration in  $|\psi\rangle_{\text{ideal}}$ .

the other, one can assume that the coupling strengths do not change during the collective dynamics observed in our manuscript. This is due to the large difference of timescales between the excited state lifetime of 30 ns and the motional period of the trapped atoms of about 10 µs. In order to model these fluctuations of the coupling strength in our numerical simulation, we assume a Gaussian probability distribution of  $\beta_f$  values,  $p(\beta_f)$ . In order to ensure that  $\beta_f$  only takes positive values, we truncate the distribution at  $\beta_f = 0$  and  $\beta_f = 1$ . We then draw a random  $\beta_f$  for each atom from this probability distribution, which is shown in Fig. S2, and propagate the light field through the ensemble of atoms using our cascaded interaction model. We repeat this process 100 times and average the resulting model predictions. We then fit the resulting model predictions to the experimental data shown in Fig. 3 of the main manuscript and obtain a fitted mean and standard deviation of  $\bar{\beta}_f = 0.0112$ and  $\sigma_{\beta_f} = 0.0065$  for the truncated Gaussian distribution, respectively. This is almost identical to the fitted values reported in our recent publication [26].

#### E. Influence of imperfect state preparation

Ideally, we want to initialize each atom in a coherent superposition between ground and excited state:

$$|\psi\rangle_{\text{ideal}} = \cos\left(\frac{A}{2}\right)|g\rangle - i\sin\left(\frac{A}{2}\right)|e\rangle.$$
 (S9)

However, both the temperature-induced fluctuations of the coupling strength,  $\beta_f$ , and the finite excitation pulse length limit the fidelity of the state preparation in our experiment. In order to study the influence of these imperfections on the collective dynamics, we compare dif-

ferent model predictions for the dynamics of the power emitted into the forward direction,  $P_f$ , as a function of pulse area, A. Figure S3 shows the model predictions for 1000 atoms for three different assumptions. In (a), we include both the temperature-induced fluctuations of the coupling strengths and the finite excitation pulse duration. This is the model prediction which we also show in the manuscript. In (b), we assume a perfectly homogeneous coupling strength. Qualitatively, the dynamics is still very similar to the one displayed in (a). In both cases, the maximal delay,  $t_D$ , is observed for a pulse area slightly larger than A, and the dynamics is asymmetric with respect to maximal inversion. However, the asymmetry is more pronounced in (b), and the maximal delay is larger. In (c), we assume that all atoms are initially prepared in  $|\psi\rangle_{\text{ideal}}$ , and that the coupling strength is constant, i.e. we neglect all experimental imperfections. There, the asymmetry with respect to full inversion is lifted, and the maximal delay occurs at a pulse area of  $\pi$ . This suggests that both the asymmetry and the fact that we observe maximal inversion for a pulse area larger than  $\pi$  are due to the finite pulse duration. We define A as the pulse area seen by the first atom of the ensemble, which is slightly larger than the average pulse area seen by the ensemble due to absorption of the excitation pulse along the ensemble. This explains why we observe maximal inversion for a pulse area that is larger than  $\pi$  [26]. The asymmetry of the time traces with respect to full inversion is due to a combination of this pulse absorption and the fact that we work with a cascaded system. There, the first atom will always emit independently, while the last atom is driven by the light emitted by the entire ensemble. For a pulse area slightly larger than  $\pi$ , the last atom is prepared closer to full inversion than the first atom, and, consequently, the superradiant burst is more pronounced than for a pulse area slightly smaller than  $\pi$ .